

Dynamics of discrete solitons in the fractional discrete nonlinear Schrödinger equation with the quasi-Riesz derivative

Ming Zhong,^{1,2} Boris A. Malomed,^{3,4} and Zhenya Yan^{1,2,*}

¹*KLMM, Academy of Mathematics and Systems Science, Chinese Academy of Sciences, Beijing 100190, China*

²*School of Mathematical Sciences, University of Chinese Academy of Sciences, Beijing 100049, China*

³*Department of Physical Electronics, School of Electrical Engineering, Faculty of Engineering, Tel Aviv University, Tel Aviv 69978, Israel*

⁴*Instituto de Alta Investigación, Universidad de Tarapacá, Casilla 7D, Arica, Chile*

We elaborate a fractional discrete nonlinear Schrödinger (FDNLS) equation based on an appropriately modified definition of the Riesz fractional derivative, which is characterized by its Lévy index (LI). This FDNLS equation represents a novel discrete system, in which the nearest-neighbor coupling is combined with long-range interactions, that decay as the inverse square of the separation between lattice sites. The system may be realized as an array of parallel quasi-one-dimensional Bose-Einstein condensates composed of atoms or small molecules carrying, respectively, a permanent magnetic or electric dipole moment. The dispersion relation (DR) for lattice waves and the corresponding propagation band in the system's linear spectrum are found in an exact form for all values of LI. The DR is consistent with the continuum limit, differing in the range of wavenumbers. Formation of single-site and two-site discrete solitons is explored, starting from the anti-continuum limit and continuing the analysis in the numerical form up to the existence boundary of the discrete solitons. Stability of the solitons is identified in terms of eigenvalues for small perturbations, and verified in direct simulations. Mobility of the discrete solitons is considered too, by means of an estimate of the system's Peierls-Nabarro potential barrier, and with the help of direct simulations. Collisions between persistently moving discrete solitons are also studied.

I. INTRODUCTION

The fractional derivative [1, 2] was originally developed as a formal generalization of the classical integer derivative. The fractional derivatives have found applications in a variety of fields of science and engineering, such as non-Gaussian random processes, fluid mechanics, quantum mechanics, optics, plasmas physics, Bose-Einstein condensates, biology, environmental sciences, materials, control theory, electrical engineering, signal and image processing, etc. (see, e.g., Refs. [3–12], books [13–19] and reviews [20–22]). There are different formal definitions of the fractional derivatives. Many mathematical works dealt with quite complex ones, such as the Riemann-Liouville [1] and Caputo fractional derivatives. The latter one is written as [2]

$$D_x^\alpha \psi(x) = \frac{1}{\Gamma(1 - \{\alpha\})} \int_0^x \frac{\psi^{(n)}(\xi)}{(x - \xi)^{\{\alpha\}}} d\xi, \quad (1)$$

where α is the non-integer order of the derivative, $n \equiv [\alpha] + 1$, $[\alpha]$ is for the integer part of the fractional order, $\{\alpha\} \equiv \alpha - [\alpha]$ is its fractional part, $\Gamma(\cdot)$ is the Gamma-function, and $\psi^{(n)}$ is the usual derivative of the integer

order n . Note that this and other definitions (see below) represents the fractional derivative as an integral (nonlocal) operator, rather than as a differential one.

In the context of physically relevant models, fractional derivatives had originally appeared as the kinetic-energy operator in the framework of *fractional quantum mechanics*, which was introduced by Laskin [5–7] (see also Ref. [23]) for nonrelativistic particles which move, at the classical level, by *Lévy flights* (random leaps), so that the mean distance $|x|$ of the particle, which moves by one-dimensional (1D) “flights” from the initial position, $x = 0$, grows with time t as

$$|x| \sim t^{1/\alpha}, \quad (2)$$

where the *Lévy index* (LI) α takes values [24]: $0 < \alpha \leq 2$. The limit value, $\alpha = 2$, corresponds to the usual Brownian random walk, while at $\alpha < 2$ Eq. (2) demonstrates that the Lévy flights give rise to faster growth of $|x|$ at $t \rightarrow \infty$.

The derivation of the effective Schrödinger equation as a result of the quantization of a particle which moves, at the classical level, by Lévy flight was performed in terms of the fundamental formalism which defines quantum mechanics by means of the Feynman's path integration. This formalism represents the quantum dynamics of a particle as a result of the superposition of virtual motions along all randomly chosen trajectories (paths). The superposition is defined as the integral in the space

*Electronic address: `{\itEmail:}zyyan@mrc.iss.ac.cn`(correspondingauthor)

of all paths, $\sim \int \exp[iS(\text{path})] d(\text{path})$, where S is the classical action corresponding to a particular path [25]. Laskin had developed this approach for the superposition of the paths which correspond not to the usual Brownian random walks, but to chains of Lévy flights. In the 1D setting, the result is the fractional linear Schrödinger (FLS) equation for wave function $\psi(x, t)$, which is written, in the scaled form, as [7, 26–29]

$$i \frac{\partial \psi}{\partial t} = \frac{1}{2} \left(-\frac{\partial^2}{\partial x^2} \right)^{\alpha/2} \psi + V(x)\psi, \quad \alpha \in (0, 2], \quad (3)$$

where $V(x)$ is the same real-valued external potential [7, 26], which appears in the usual Schrödinger equation. The external potential may also be chosen as a complex \mathcal{PT} -symmetric one [29].

A result of the derivation of Eq. (3) by means of the path-integral formalism is that the usual kinetic-energy operator, $-(1/2)\partial^2/\partial x^2$, which corresponds to $\alpha = 2$, is replaced in Eq. (3), at $\alpha < 2$, by the fractional *Riesz derivative* [30]. Its definition is more straightforward than that of the abstract Caputo derivative (1), being composed as the juxtaposition of the direct and inverse Fourier transforms ($x \rightarrow p \rightarrow x$) of the wave function,

$$\left(-\frac{\partial^2}{\partial x^2} \right)^{\alpha/2} \psi(x) = \frac{1}{2\pi} \int_{-\infty}^{+\infty} dp |p|^\alpha \int_{-\infty}^{+\infty} d\xi e^{ip(x-\xi)} \psi(\xi). \quad (4)$$

This definition implies that the action of the fractional derivative, $(-\partial^2/\partial x^2)^{\alpha/2}$, in the Fourier space amounts to the straightforward multiplication: $\hat{\psi}(p) \rightarrow |p|^\alpha \hat{\psi}(p)$, where

$$\hat{\psi}(p) = \int_{-\infty}^{+\infty} \exp(-ipx) \psi(x) dx \quad (5)$$

is the Fourier transform of the wave function. In definition (4), α is the same LI which determines the Lévy flights as per Eq. (2).

The next step in the development of models originating from fractional mechanics is to consider Bose-Einstein condensates (BECs) in an ultracold gas of particles moving by Lévy flights [31–33]. It is commonly known that, in the framework of the mean-field theory, the usual BEC is governed by the Gross-Pitaevskii (GP) equation for the single-particle wave function ψ , with the cubic term which represents effects of inter-particle collisions [34]. While a systematic derivation of the respective *fractional* GP (FGP) equation remains to be elaborated, it is natural to expect that it will take the form of the GP equation with the kinetic-energy operator replaced by its fractional counterpart defined as per Eqs. (4). In the scaled form, the equation will take the form of the respective fractional nonlinear Schrödinger (FNLS, alias FGP) equation [35–44],

$$i \frac{\partial \psi}{\partial t} = \frac{1}{2} \left(-\frac{\partial^2}{\partial x^2} \right)^{\alpha/2} \psi + V(x)\psi + \sigma |\psi|^2 \psi, \quad (6)$$

where $\sigma = +1$ or -1 corresponds, respectively, to the repulsive or attractive inter-particle collisions in the ultracold gas [31, 32], and $V(x)$ is a real-valued external potential, or complex \mathcal{PT} -symmetric potential [35, 41–44]. Available techniques make it possible to produce reliable numerical solutions of the FNLS equations [45].

Thus far, no experimental demonstration of the fractional quantum mechanics or the corresponding fractional BEC has been reported. A more promising physical realization of fractional Schrödinger equation is suggested by the commonly known similarity of the Schrödinger equation and the propagation equation for the amplitude of the optical field in the usual case of paraxial diffraction, with time t replaced, as the evolutionary variable, by the propagation distance, z [46]. A scheme for the realization of this possibility was proposed by Longhi [26], who considered the transverse light dynamics in an optical cavity incorporating two lenses and a phase mask, which is placed in the middle (Fourier) plane. The lenses perform the direct and inverse Fourier transforms of the light beam with respect to the transverse coordinate, which are ingredients of the definition of the Riesz derivative in Eq. (4). Further, according to Eq. (4), the action of the fractional diffraction on the Fourier transform (5) of the optical amplitude amounts to the phase shift,

$$\hat{\psi}(p) \rightarrow \hat{\psi}(p) \exp(i|p|^\alpha Z), \quad (7)$$

where Z is the propagation distance which accounts for the fractional diffraction. The corresponding differential phase shift of the Fourier components is imposed by the phase mask placed in the midplane of the optical cavity. The required mask can be created as a computer-generated hologram [47].

The setup which is outlined above provides a single-step transformation of the optical beam. The continuous FNLS equation is then introduced as an approximation for many cycles of circulation of light in the cavity, assuming that each cycle introduces a small phase shift (7), while the cubic term in the equation represents the Kerr nonlinearity of the optical material.

An interesting ramification of the recently published theoretical works on the topic of fractional media is the study of their discrete counterparts [48–53], which are of nonlocal type. In particular, Ref. [49] provided a theoretical proof for the existence of onsite and offsite fractional-order discrete solitary waves, encompassing a discussion on the Peierls-Nabarro potential barrier (PNPB). However, in those works, discrete fractional derivatives were defined in a complex form, as a discrete version of the Riemann-Liouville fractional derivative for the continuous field [1]. We here aim to define a new discrete fractional derivative in an essentially simpler form, following the pattern of the continuous Riesz derivative (4). Our fractional discrete NLS (FDNLS) equation is introduced

in Section 2, where we also demonstrate its physical realization, in the form of a system of GP equations for an array of parallel chains of dipolar BECs. Some results, such as the dispersion relation (DR) for the lattice waves, along with the corresponding band in the system's linear spectrum (for all values of the respective Lévy index (LI)), and strongly localized single- and double-site discrete solitons in the anticontinuum limit (AL), are obtained in an analytical form. Systematic numerical results for the structure and stability of families of the discrete solitons, which originate, as the single- and double-site ones in the AL approximation and are extended numerically up to their existence boundaries, are reported in Section 3. In particular, we find that the family of in-phase double-site discrete solitons is completely unstable, while the family of out-of-phase ones includes a stable segment. Mobility of the discrete solitons and collisions between mobile ones are considered in Section 4. In particular, the mobility is predicted through the consideration of the respective Peierls-Nabarro potential barrier (PNPB). The work is concluded by Section 5.

II. THE FRACTIONAL DISCRETE NLS MODEL

A. The formulation of the model with quasi-Riesz fractional derivative

A complex lattice function u_n of the discrete coordinate, $n = 0, \pm 1, \pm 2, \pm 3, \dots$, is represented by its Fourier transform, $U(k)$, which is defined in interval $k \in [-\pi, +\pi]$ as a periodic function of real wavenumber k in the Fourier space. The direct and inverse relations between u_n and $U(k)$ are

$$u_n = \frac{1}{2\pi} \int_{-\pi}^{+\pi} U(k) e^{ikn} dk, \quad U(k) = \sum_{n=-\infty}^{+\infty} u_n e^{-ikn}. \quad (8)$$

In terms of the Fourier transform of continuous functions, the direct counterpart of the Riesz fractional derivative, with Lévy index $\alpha \in (1, 2]$, of the complex discrete function u_n can be derived as follows:

$$\begin{aligned} \left(-\frac{\widehat{\partial}^2}{\partial n^2}\right)^{\alpha/2} u_n &\equiv \frac{1}{2\pi} \int_{-\pi}^{+\pi} dk \left(e^{ikn} |k|^\alpha \sum_{m=-\infty}^{+\infty} u_m e^{-ikm} \right) \\ &= \frac{1}{\pi} \sum_{m=-\infty}^{+\infty} u_m \int_0^\pi \cos((m-n)k) \cdot k^\alpha dk \\ &= \sum_{\ell=-\infty}^{+\infty} D_\ell^{(\alpha)} u_{n+\ell}, \end{aligned} \quad (9)$$

where the intersite coupling coefficients are

$$\begin{aligned} D_\ell^{(\alpha)} = D_{-\ell}^{(\alpha)} &= \frac{1}{\pi} \int_0^\pi \cos(\ell k) \cdot k^\alpha dk \\ &= -\frac{\alpha}{\pi \ell} \int_0^\pi \sin(\ell k) k^{\alpha-1} dk \end{aligned} \quad (10)$$

(the latter expression, obtained by means of the integration by parts, is more convenient for the subsequent analysis; obviously, the expression (10) vanishes, as it should, for all $\ell \neq 0$ at $\alpha = 0$). Note that the notation for the novel fractional derivative of the lattice function u_n , $\left(-\frac{\widehat{\partial}^2}{\partial n^2}\right)^{\alpha/2} u_n$, given by Eq. (9), is symbolic, differing from the standard definition in the continuum limit (4). Similarly, the Fourier transform was also utilized to give another discrete version for fractional derivatives [54–56].

As a result, the definition given by Eq. (9) introduces a new family of fractional discrete systems for $\alpha \leq 2$. In the limit case of $\alpha = 2$ (non-fractional diffraction), the discrete diffraction operator includes coupling between non-neighboring sites, taking the form of

$$\left(-\frac{\widehat{\partial}^2}{\partial n^2}\right) u_n = \frac{\pi^2}{3} u_n + 2 \sum_{\ell \in \mathbb{Z} \setminus \{0\}} (-1)^\ell \ell^{-2} u_{n+\ell}. \quad (11)$$

The difference of Eq. (11) from the finite-difference operator of the coupling between nearest neighbors, adopted in the commonly known DNLS equation (see Eq. (24) below) [57–59], is explained by the fact that the usual operator is obtained by first taking $\alpha \rightarrow 2$ in the continuum FNLS equation, and then applying the straightforward discretization to the resulting NLS equation. Operator (11) is derived differently: first, the discretization is applied to the continuum FNLS equation, and then the limit of $\alpha \rightarrow 2$ is taken in it. Thus, we conclude that the two limit procedures *do not commute*, which explains the difference of the operator (11) from the straightforward finite difference. In fact, the different discretization of the second-order derivative that we consider here is a spectral format of the discretization [60], which is thus a global format, in contrast to finite differences.

For arbitrary α , the integral in Eq. (10) can be formally expressed in terms of the incomplete Gamma-function, but this is useless for practical applications, making it necessary to compute coefficients $D_\ell^{(\alpha)}$ numerically. For $\alpha < 1$, the asymptotic form of the coupling coefficients at $|\ell| \rightarrow \infty$ is

$$D_\ell^{(\alpha)} \approx -\frac{\alpha \Gamma(\alpha)}{\pi |\ell|^{\alpha+1}} \sin\left(\frac{\pi}{2} \alpha\right). \quad (12)$$

For $\alpha > 1$, a similar formula is

$$D_\ell^{(\alpha)} \approx \frac{(-1)^\ell \alpha}{\pi^{2-\alpha} \ell^2}. \quad (13)$$

Expression (9) takes a much simpler form in the special case of $\alpha = 1$:

$$\left(-\frac{\widehat{\partial}^2}{\widehat{\partial}n^2}\right)^{1/2} u_n = \frac{\pi}{2} u_n - \frac{2}{\pi} \sum_{\ell=-\infty}^{+\infty} \frac{u_{n+2\ell+1}}{(2\ell+1)^2}. \quad (14)$$

Note that Eq. (14) includes the coupling of a given site, n , to ones $n\pm 1, n\pm 3, n\pm 5, \dots$, but not $n\pm 2, n\pm 4, n\pm 6, \dots$. The ‘‘self-coupling’’ term $\frac{\pi}{2} u_n$ in Eq. (14) is tantamount to a shift of the propagation constant.

Thus, based on the defined discrete quasi-Riesz fractional derivative (9), we introduce the novel fractional discrete NLS (FDNLS) equation

$$i \frac{du_n}{dt} = C \left(-\frac{\widehat{\partial}^2}{\widehat{\partial}n^2}\right)^{\alpha/2} u_n - \sigma |u_n|^2 u_n, \quad (15)$$

whose actual form is

$$i \frac{du_n}{dt} = C \sum_{\ell=-\infty}^{+\infty} D_\ell^{(\alpha)} u_{n+\ell} - \sigma |u_n|^2 u_n, \quad (16)$$

where $C > 0$ is the coefficient of the fractional discrete diffraction or the linear coupling strength between adjacent sites of the lattice, and $\sigma = +1$ or -1 represent the self-focusing or defocusing nonlinearity, respectively. Note that the cubic nonlinear term may be replaced by different ones [58, 59], such as the cubic-quintic term, $g_1 |u_n|^2 u_n + g_2 |u_n|^4 u_n$, the power-law nonlinearity, $|u_n|^{2p} u_n$, and the saturable expression, $u_n / (1 + |u_n|^2)$. Similar to its continuum counterpart, Eq. (15) conserves the Hamiltonian (energy) and power (norm),

$$H = \sum_n \left[C u_n^* \left(-\frac{\widehat{\partial}^2}{\widehat{\partial}n^2}\right)^{\alpha/2} u_n - \frac{\sigma}{2} |u_n|^4 \right], \quad (17)$$

$$P = \sum_n |u_n|^2, \quad (18)$$

where the star denotes the complex conjugate. The conservation of the Hamiltonian and power corresponds, respectively, to the invariance of Eq. (16) with respect to the time translation and phase shift. Note that we can also consider the FDNLS Eq. (15) with a real or complex (e.g., \mathcal{PT} -symmetric) potential $V(n)$,

$$i \frac{du_n}{dt} = C \left(-\frac{\widehat{\partial}^2}{\widehat{\partial}n^2}\right)^{\alpha/2} u_n + V(n) u_n - \sigma |u_n|^2 u_n. \quad (19)$$

As $\sigma = 0$, Eq. (19) becomes the fractional discrete version of the continuous FLS Eq. (3)

$$i \frac{du_n}{dt} = \frac{1}{2} \left(-\frac{\widehat{\partial}^2}{\widehat{\partial}n^2}\right)^{\alpha/2} u_n + V(n) u_n. \quad (20)$$

In particular, at $\alpha = 1$, the cases of $\sigma = +1$ and -1 for Eq. (15) are mutually equivalent, as the latter case may be cast into the former one by means of the well-known *staggering transform*: the substitution of

$$u_n(t) \equiv (-1)^n q_n^*(t) e^{-iC\pi t}, \quad (21)$$

where $*$ stands for the complex conjugate, in Eq. (14) replaces it (after the application of the complex conjugation) by the the same equation for variables $q_n(t)$, but with $\sigma \rightarrow -\sigma$. Thus, it is sufficient to consider only $\sigma = +1$ in the case of $\alpha = 1$. The staggering transform does not apply to Eq. (16) in the general case of $\alpha \neq 1$.

For $\alpha = 2$, the FDNLS equation (15) reduces to a novel integer-order DNLS equation

$$i \frac{du_n}{dt} = C \left(-\frac{\widehat{\partial}^2}{\widehat{\partial}n^2}\right) u_n - \sigma |u_n|^2 u_n. \quad (22)$$

According to the definition of discrete derivative given by Eq. (11), the explicit form of Eq. (22) is

$$i \frac{du_n}{dt} = C \left(\frac{\pi^2}{3} u_n + 2 \sum_{\ell \in \mathbb{Z} \setminus \{0\}} \frac{(-1)^\ell}{\ell^2} u_{n+\ell} \right) - \sigma |u_n|^2 u_n, \quad (23)$$

which, as stressed above, differs from the usual DNLS equation [57–59]:

$$i \frac{du_n}{dt} = C(2u_n - u_{n+1} - u_{n-1}) - \sigma |u_n|^2 u_n. \quad (24)$$

B. Discrete standing-wave solutions and their stability

In what follows below, we consider stationary solutions of Eq. (16) and their stability. First, we look for standing-wave solutions to Eq. (16) with $\sigma = 1$ in the form of

$$u_n(t) = v_n e^{-i\omega t}, \quad (25)$$

with real frequency ω and stationary amplitudes v_n satisfying the steady-state equation

$$\left(|v_n|^2 + \omega\right) v_n = C \sum_{\ell=-\infty}^{+\infty} D_\ell^{(\alpha)} v_{n+\ell}. \quad (26)$$

Note that $\omega < 0$ can be scaled out from Eq. (26) by means of the scaling transformation

$$v_n = \sqrt{-\omega} \hat{v}_n, \quad C = -\omega \hat{C}, \quad (27)$$

therefore we fix $\omega = -1$, keeping coupling constant C as the control parameter. In our numerical calculations, Eq. (9) is truncated from $\ell = -100$ to $+100$.

Once standing-wave solutions of Eq. (26) have been found, their linear stability is addressed by means of the

Bogoliubov-de Gennes linearized equations for small perturbations. To this end, expressions for the perturbed solutions with an infinitesimal amplitude δ of the perturbations are substituted in Eq. (15) as

$$u_n(t) = e^{-i\omega t} \left[v_n + \delta \left(a_n e^{\lambda t} + b_n^* e^{\lambda^* t} \right) \right] \quad (28)$$

with $\lambda \in \mathbb{C}$, $(a_n, b_n) \in \mathbb{C}^2[n]$, $n \in \mathbb{Z}$, which gives rise to the eigenvalue problem

$$\begin{pmatrix} L_{11} & L_{12} \\ -L_{12}^* & -L_{11}^* \end{pmatrix} \begin{pmatrix} a_n \\ b_n \end{pmatrix} = i\lambda \begin{pmatrix} a_n \\ b_n \end{pmatrix} \quad (29)$$

with

$$L_{11} = C \left(-\frac{\widehat{\partial}^2}{\widehat{\partial} n^2} \right)^{\alpha/2} - 2|v_n|^2 - \omega, \quad (30)$$

$$L_{12} = -v_n^2.$$

The discrete soliton $u_n(t)$ is unstable if there exists λ with $\text{Re}(\lambda) > 0$. Predictions for the linear stability are then verified by direct simulations of the perturbed evolution, by dint of the fourth-order Runge-Kutta method [61], monitoring the conservation of Hamiltonian (17) and power (18) to validate the accuracy of the numerical scheme.

C. Implementation of the model in an array of dipolar BECs

The fractional discrete nonlinear model which is based on Eq. (16) with the intersite coupling defined, for $\alpha = 2$, by Eq. (22), can be implemented as an array of parallel quasi-one-dimensional (quasi-1D) traps for the Bose-Einstein condensate (BEC) of atoms carrying a permanent magnetic dipolar moment [62], or the condensate of small polar molecules with a permanent electric dipolar moment (cf. Ref. [63]). Indeed, the energy density for the interaction between two parallel 1D chains of dipoles separated by distance L can be easily found,

$$\mathcal{E} = -\frac{m_1 m_2}{2\pi L^2} \sin \theta_1 \cdot \sin \theta_2, \quad (31)$$

where $m_{1,2}$ are dipolar densities in the two chains, $\theta_{1,2}$ are fixed angles between the dipoles in each chain and its direction, and the magnetic permeability or electric permittivity of vacuum is set to be 1.

The fractional discrete model similar to the ones considered here corresponds to the setup with the array of parallel quasi-1D traps uniformly filled by the dipolar BEC, the discrete coordinate n in Eq. (16) being the number of the trap in the array. Then, in the case of $m_1 = m_2$ and $\theta_1 = -\theta_2$, Eq. (31) exactly corresponds to the set of the coupling coefficients (11) and (13). Relation $\theta_1 = -\theta_2$ implies that the dipolar polarization is

imposed by an external magnetic or electric field with a periodically flipping spatial structure. One can also consider the system with unequal dipole moments in the two chains, i.e., $m_1 \neq m_2$ and/or $\theta_1 \neq \theta_2$. It will be described by a model similar to Eq. (16), but with the intersite interaction subjected to spatially periodic modulation. On the other hand, Eqs. (12) and (14) represent theoretical models which cannot be directly implemented by means of the physical setting outlined here.

D. The dispersion relation (DR) and spectral band for linear modes

Fundamental characteristics of a discrete system is the dispersion relation (DR) between real frequency ω and wavenumber k of small-amplitude lattice waves (“phonons”) governed by the linearized system, and the spectral band (interval) of frequencies admitting the propagation of the linear waves [57]. To identify the DR, the solution of the linearized equation (26) is looked for as $v_n \sim \exp(ikn)$, which yields

$$\omega(k) = C \sum_{\ell=-\infty}^{+\infty} D_{\ell}^{(\alpha)} \cos(\ell k). \quad (32)$$

As it follows from definition (10) of coefficients $D_{\ell}^{(\alpha)}$ in terms of the Fourier integral, Eq. (32) is tantamount to a simple result,

$$\omega(k) = C|k|^{\alpha}, \quad (33)$$

Notice that the discrete DR (33) is similar to the dispersion relation in the continuous case, except for the range of wavenumber k . For $\alpha = 2$, the DR of the integer-order discrete Eq. (23) is $\omega(k) = Ck^2$, which differs from the usual DNLS equation (24) whose DR is $\omega(k) = 2C(1 - \cos(k))$.

The particular cases of Eq. (32), *viz.*,

$$\omega(k=0) = C \sum_{\ell=-\infty}^{+\infty} D_{\ell}^{(\alpha)} = 0, \quad (34)$$

and

$$\omega(k=\pi) = C \sum_{\ell=-\infty}^{+\infty} (-1)^{\ell} D_{\ell}^{(\alpha)} = C\pi^{\alpha}, \quad (35)$$

can be readily checked directly, using the known formulas

$$\sum_{\ell=1}^{\infty} \ell^{-1} \sin(\ell k) = (\pi - k)/2, \quad (36)$$

and

$$\sum_{\ell=1}^{\infty} (-1)^{\ell} \ell^{-1} \sin(\ell k) = -k/2, \quad (37)$$

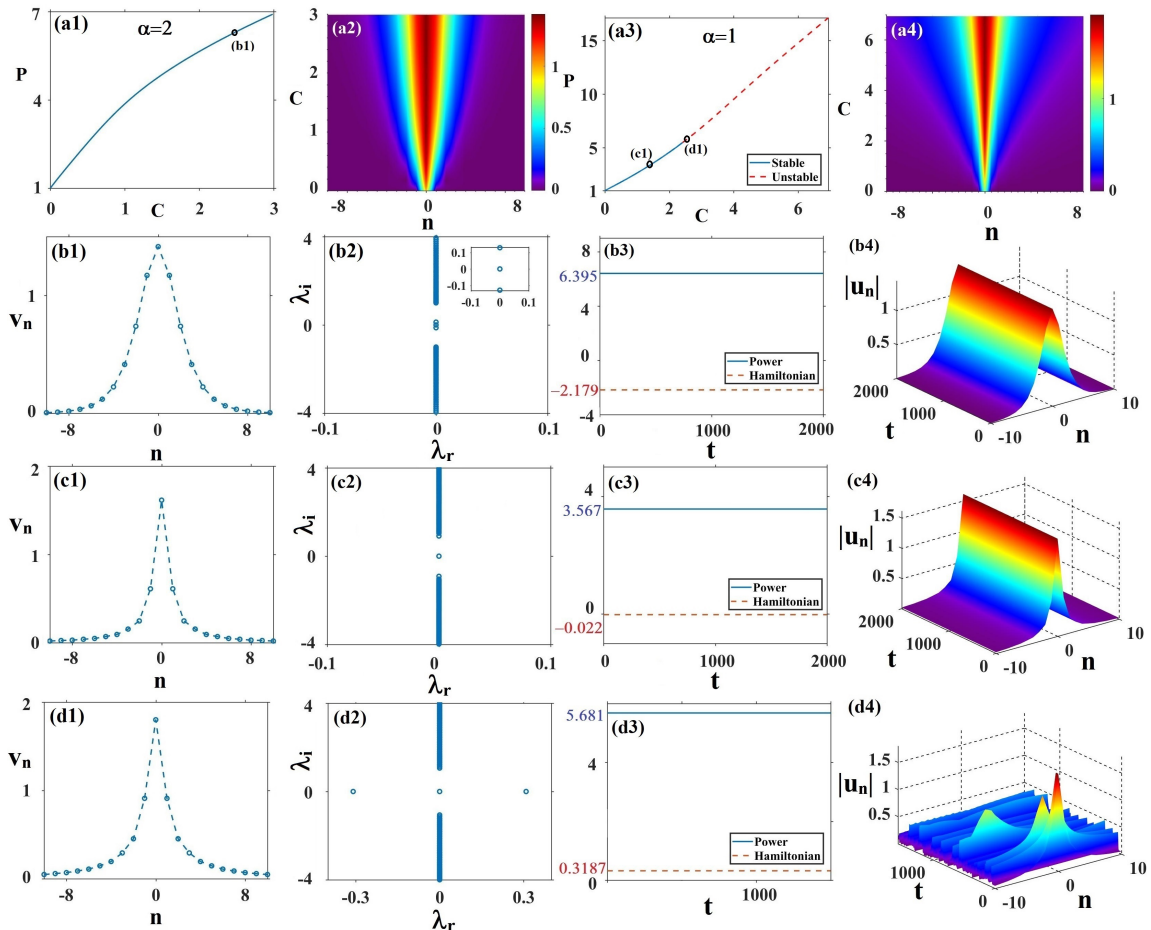


FIG. 1: The single-site mode. The dependence of power P on coupling constant C as produced by the numerical solution of Eq. (26) with (a1) $\alpha = 2$ and (a3) $\alpha = 1$. The solid and dashed lines represent stable and unstable discrete solitons, respectively. Labels (b1,c1,d1) correspond to discrete solitons displayed in panels (b1,c1,d1). The variation of profiles v_n , following the increase of coupling constant C are displayed for $\alpha = 2$ (a2) and $\alpha = 1$ (a4). The second row, from left to right, displays the profiles of discrete soliton (b1), linear spectrum (b2), power and Hamiltonian in the course of the propagation (b3), and the nonlinear dynamical behaviour (b4) for $\alpha = 2, C = 2.5$. The power and Hamiltonian are represented by solid and dashed lines, respectively. The third and fourth rows are the same as the second one, but with parameters $\alpha = 1, C = 1.5$ and $\alpha = 1, C = 2.5$, respectively.

which are valid for $0 \leq k \leq \pi$ (note that the values produced by Eqs. (36) and (37) at $k = 0$ and $k = \pi$ are realized as limit values of these expressions for $k \rightarrow 0+$ and $\pi - k \rightarrow 0$, respectively). Thus, the lattice band, bounded by the bottom and top points (34) and (35) of the DR, is

$$0 \leq \omega \leq C\pi^\alpha. \quad (38)$$

Discrete solitons may exist in the form of Eq. (25) at frequencies which do not belong to the band. Indeed, it can be checked that intrinsic frequencies of all the discrete solitons reported below are located outside of the band.

Note also that DR (33) gives rise to a singularity of the group velocity,

$$V_{gr} = d\omega/dk = C\alpha|k|^{\alpha-1}\text{sgn}(k), \quad (39)$$

and of the respective dispersion coefficient, $d\omega/dk$, at $k \rightarrow 0$ for $\alpha \leq 1$. This fact implies decay of propagating lattice pulses in the latter case.

E. The anti-continuum limit for discrete solitons

It is well known that the anti-continuum (AC) limit, corresponding to $C \rightarrow 0$ in Eq. (15), offers a convenient starting point for constructing various solutions of DNLS equations [57, 64–70]. In this limit, the sites u_n are decoupled, hence Eq. (26) amounts to a simple equation which should be solved independently at each site:

$$\left(|v_n|^2 - 1\right)v_n = 0. \quad (40)$$

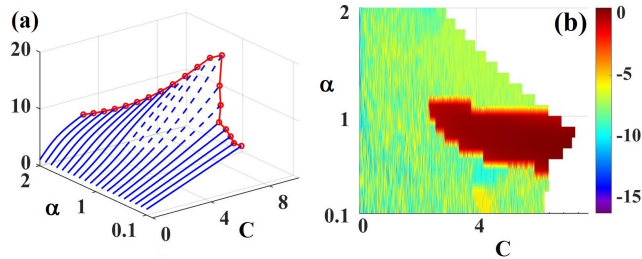


FIG. 2: The single-site mode. (a) The dependence of power P on coupling constant C and Lévy index α , where solid and dashed lines denote stable and unstable segments, respectively. The red circle denotes the boundary value of C above which the discrete solitons do not exist. (b) The largest real part λ_r of the linear eigenvalues produced by the numerical solution of Eq. (29) is charted in the (C, α) plane. The boundary of the chart corresponds to the chain of red circles in panel (a). The color bar denotes values $\log(\max\{|\text{Re}(\lambda)|\})$, e.g., “-5” corresponds to $\max\{|\text{Re}(\lambda)|\} = 10^{-5}$ (actually, extremely small values imply stability of the stationary mode).

Obviously, its solutions are $v_n = 0$, or $v_n = \exp(i\theta_n)$ with phase θ_n being a free parameter for each site. Then, the crucial issue is what set of values of the phases at different sites continues to a true solution at small nonzero values of the coupling constant C . Indeed, according to the MacKay-Aubry’s theorem [64], discrete solitons of Eq. (16) with $C = 0$ and $v_n = \pm 1$, or 0 can be continued from the AC limit to finite values of C , provided that the frequency ω does not resonate with linear modes of the system.

While our fractional DNLS model (15) is consistent with the usual DNLS equation (24) in the AC limit, the linear spectra of our model are strongly different, see below. In particular, substitution of $C = 0$ in Eq. (29) leads to the following eigenvalue problem:

$$\begin{aligned} (1 - 2v_n^2) a_n - v_n^2 b_n &= i\lambda a_n, \\ v_n^2 a_n - (1 - 2v_n^2) b_n &= i\lambda b_n, \end{aligned} \quad (41)$$

where $n \in \mathbb{Z}$, and the limit solution can be chosen to be real-valued. Supposing that it includes N excited sites with $v_n = \pm 1$ and $v_n = 0$ at other sites in the AC limit, a direct solution of Eq. (41) produces N pairs of zero eigenvalues, together with an infinite number of eigenvalues $\lambda = \pm i$. According to the discrete Sturm-Liouville theorem [71] and regular perturbation theory [72], the infinite set of the eigenvalues is converted into the continuous spectrum near $\lambda = \pm i$ at small finite values of C , without producing any unstable eigenvalues with $\text{Re}(\lambda) > 0$. As for the N pairs of zero eigenvalues, the invariance with respect to the phase shift keeps one pair of exact zero eigenvalues at $C > 0$. The critical issue for the stability analysis is to identify $N - 1$ eigenvalue pairs which had $\lambda = 0$ at $C = 0$, and become nonzero at $C > 0$.

III. DISCRETE SOLITONS: FORMATION AND STABILITY

In what follows, the existence and stability of discrete solitons are studied numerically. We mainly focus on the discrete solitons coded by a sequence $\beta_n = \{0, +, -\}$, $n \in \mathbb{Z}$ excited on $N = 1$ or 2 sites (cf. Ref. [69]), where $\beta_n = \{0, +, -\}$ indicates the values $v_n = 0$ or ± 1 in the AC limit.

A. Single-site excitations

We start the analysis with discrete solitons originating from the single-site ($N = 1$, alias onsite-centered) excitation in the AC limit. Generic examples of discrete solitons for Lévy indices $\alpha = 2$ and $\alpha = 1$ are presented in Fig. 1. Results for the fundamental discrete solitons produced by the numerical solution of Eq. (26) with $\alpha = 2$ and $\alpha = 1$ are summarized in Figs. 1(a1) and (a3), respectively, in the form of dependence $P(C)$. It is worthy to note that, unlike the case of the nearest-neighbor interaction [57, 65], the presence of the long-range coupling here does not allow the single-site discrete soliton to proceed from the AC limit to the continuum limit, even though the shape of the mode is very close to the one in the continuum form. This situation is similar to that known for discrete solitons in the recently considered fractional Frenkel-Kontorova model [73]. The critical value of coupling constant C above which no discrete soliton can be found is $C_{\text{cr}}(\alpha = 2) = 2.9820$ and $C_{\text{cr}}(\alpha = 1.0) = 6.9390$. The variation of profiles v_n , following the increase of coupling constant C are displayed at Figs. 1(a2) and (a4), respectively. One can observe that the discrete soliton with $\alpha = 2$ is localized stronger than its counterparts with $\alpha = 1.0$, which is a manifestation of the existence of power-law tails in the case of the long-range interaction [73, 74], similar to the continuum FNLS equation [45].

We have found that all discrete solitons are stable for $\alpha = 2$, which is the same as in the case of the nearest-neighbor interaction [57, 65]. However, for $\alpha = 1$ the discrete solitons become unstable above the respective critical value of the coupling constant. The instability is related to the fact that, in the framework of the continuum FNLS equation with $\alpha = 1$ the solitons are destabilized by the critical collapse [45]. Several profiles of discrete solitons are displayed in Figs. 1(b1,c1,d1). It is seen in Fig. 1(b2) that the discrete soliton with $\alpha = 2$, $C = 2.5$ displayed in Fig. 1(b1) is a linearly stable mode. The spectrum of the eigenvalues, displayed in the latter panel, contains a double zero eigenvalue, which is due to the invariance with respect to the phase shift. The simulated evolution, displayed in Fig. 1(b4) with random noise added to the initial condition, verifies the stability predicted by the linear spectrum, the accuracy of the

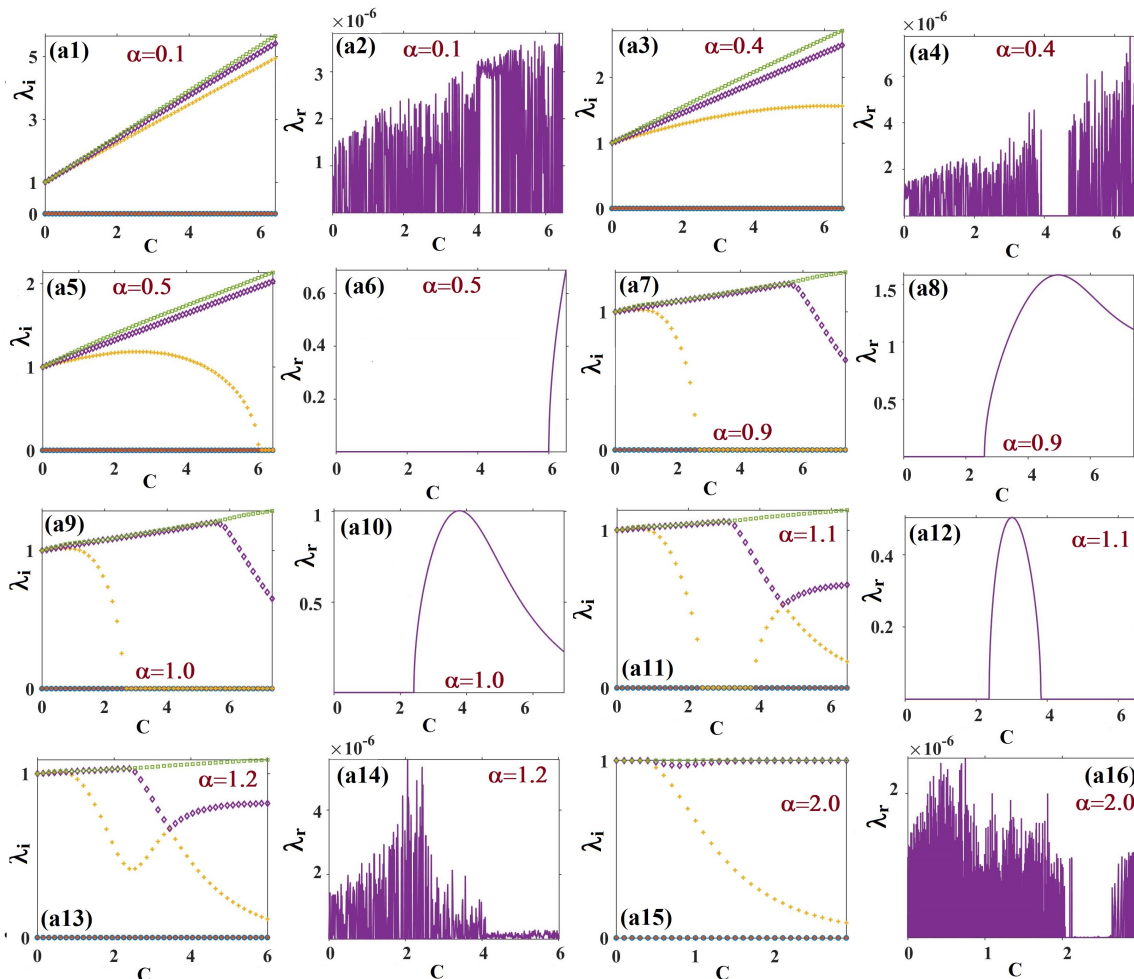


FIG. 3: The single-site mode. Critical eigenvalues (including real and imaginary parts) are produced by the numerical solution of Eq. (29) with different Lévy indices α . The five eigenvalues with the smallest imaginary parts are labeled as follows: circles, crosses, pluses, diamonds, and squares. Several spectra with positive imaginary parts and the corresponding real parts are shown, *viz.*, (a1,a2): $\alpha = 0.1$; (a3,a4): $\alpha = 0.4$; (a5,a6): $\alpha = 0.5$; (a7,a8): $\alpha = 0.9$; (a9,a10): $\alpha = 1.0$; (a11,a12): $\alpha = 1.1$; (a13,a14): $\alpha = 1.2$; (a15,a16): $\alpha = 2.0$.

simulations being confirmed by the conservation of the Hamiltonian and power in Fig. 1(b3).

Next, we examine the stability of the discrete soliton for $\alpha = 1.0$, $C = 1.5$, as shown in Fig. 1(c1). The linear spectra and direct simulations indicate that the discrete soliton is completely stable, see Figs. 1(c2,c3,c4)). Lastly, we consider the discrete soliton with $\alpha = 1.0$, $C = 2.5$ displayed in Fig. 1(d1). One observes in Fig. 1(d2) that this discrete soliton is linearly unstable, with the unstable eigenvalues bifurcating from the bottom of the continuous spectrum, cf. Refs. [57, 68, 70]. The direct simulations confirm the instability of this discrete soliton, see Figs. 1(d3,d4).

A more detailed study of the dependence of power P on the coupling constant C and Lévy index α is presented in Fig. 2(a). It is seen in Fig. 2(a) that the critical value of the coupling constant C , which is the existence boundary for the discrete solitons, decreases with the growth

of α at $\alpha \geq 0.7$, while the results for $\alpha < 0.7$ may be affected by the finite size of the underlying lattice and boundary conditions. The largest real part of the linear eigenvalue produced by Eq. (29) is shown in the (C, α) plane in Fig. 2(b), which shows that the discrete solitons are unstable only when $0.5 \leq \alpha \leq 1.1$, with C exceeding a certain threshold value.

In an attempt to explore reasons for the generation of the instability, we consider in detail the critical eigenvalues, which determine the stability, by means of the numerical solution of Eq. (29), following the variation of Lévy index α . It is relevant to mention that, in the continuum limit (in the model with the fractional and non-fractional diffraction alike), in addition to the above-mentioned invariance with respect to the phase shift, the invariance against the spatial translation gives rise to an additional pair of zero eigenvalues, hence their total number is four. We present some generic examples in Fig. 3.

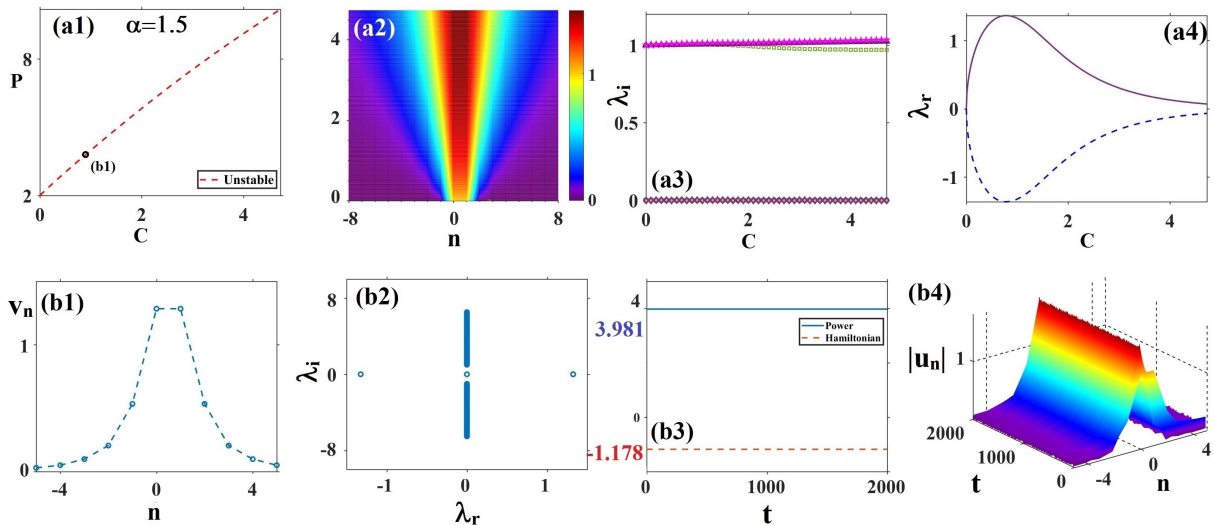


FIG. 4: Unstable two-site in-phase modes at $\alpha = 1.5$ and $C = 1$. (a1) Power P vs. the coupling constant C , as produced by the numerical solutions of Eq. (26). Label (b1) corresponds to the discrete solitons displayed in panel (b1). (a2) The variation of profiles v_n , following the increase of C . (a3,a4) Critical eigenvalues (including their real and imaginary parts), produced by the numerical solution of Eq. (29). The seven eigenvalues with the smallest imaginary parts are labeled in panel (a3) as follows: circles, crosses, plus signs, diamonds, squares, upward-pointing triangles, and five-pointed stars. The solid and dashed lines in panel (a4) represent unstable eigenvalues branching out from the original. The bottom row of panels: the profile of the discrete soliton (b1), the spectrum of eigenvalues for small perturbations about the discrete soliton (b2), the evolution of the discrete soliton's power and Hamiltonian in the course of the perturbed propagation (b3), and the corresponding evolution of the weakly unstable discrete soliton (b4).

When $0.1 \leq \alpha < 0.4$, there is a single pair of zero eigenvalues, and no eigenvalues bifurcate from the bottom edge of the continuous spectrum, see Fig. 3(a1). Further, no unstable eigenvalues appear with the increase of the coupling constant C , see Fig. 3(a2). When $\alpha = 0.4$, one observes in Fig. 3(a3) that the translation eigenvalues bifurcate from the continuous spectrum with the increase of C . They move along the imaginary axis, maintaining the linear stability, see Fig. 3(a4). A phenomenon presented in Fig. 3(a5), which is similar to that produced by the DNLS equation with saturable nonlinearity [75–77], is that the translation eigenvalue emerges from the band edge of the continuous spectrum at $\alpha = 0.5$. It vanishes at $C = 6.01$, then becoming real and expanding along the real axis, which results in instability, as seen in Fig. 3(a6). Another critical value of the Lévy index is $\alpha = 0.9$, in which case another pair of eigenvalues bifurcate from the lower edge of the continuous spectrum, see Figs. 3(a7,a8). Simultaneously, the translational eigenvalues (real ones) decrease with the generation of the above-mentioned pair. Similar results are observed at $0.9 \leq \alpha < 1.1$, see Figs. 3(a9,a10). An intriguing phenomenon occurs at $\alpha = 1.1$ is displayed in Fig. 3(a11), where the translation eigenvalue first bifurcates from the continuous spectrum, then expands along the real axis, and finally decreases due to the presence of other separate eigenvalues. After returning to the origin, this eigenvalue spreads out along the imaginary axis, and collides with

the point spectrum branching off from the continuous spectrum mentioned above. The collision is followed by the motion of the two eigenvalues in the opposite directions. Note that such a collision does not create unstable eigenvalues [78]. The corresponding changes in the real part of the eigenvalues are visualized in Fig. 3(a12). Note that the motion of the two eigenvalues in the opposite direction after the collision is inevitable, as can be deduced from the spectral distribution in the continuum limit. When α increases to 1.2, before the translation eigenvalues hit the origin, another pair of eigenvalues branches off from the continuous spectrum, therefore no unstable eigenvalues are generated. Similar collision phenomena are observed in Figs. 3(a13,a14). When α increases to 2, as shown in Figs. 3(a15,a16), no collisions are observed, and the eigenvalues branching off from the continuous spectrum undergo a recurrence in which the translation eigenvalues extend all the way along the imaginary axis without touching the origin. This scenario is also different from those known in the case of the nearest-neighbor DNLS equation, in which the eigenvalues are known to collide [57, 68].

B. Two-site excitations

Next we consider discrete solitons which are seeded, in the AL limit, by an excitation localized on a pair of adjacent sites. According to the phase difference be-

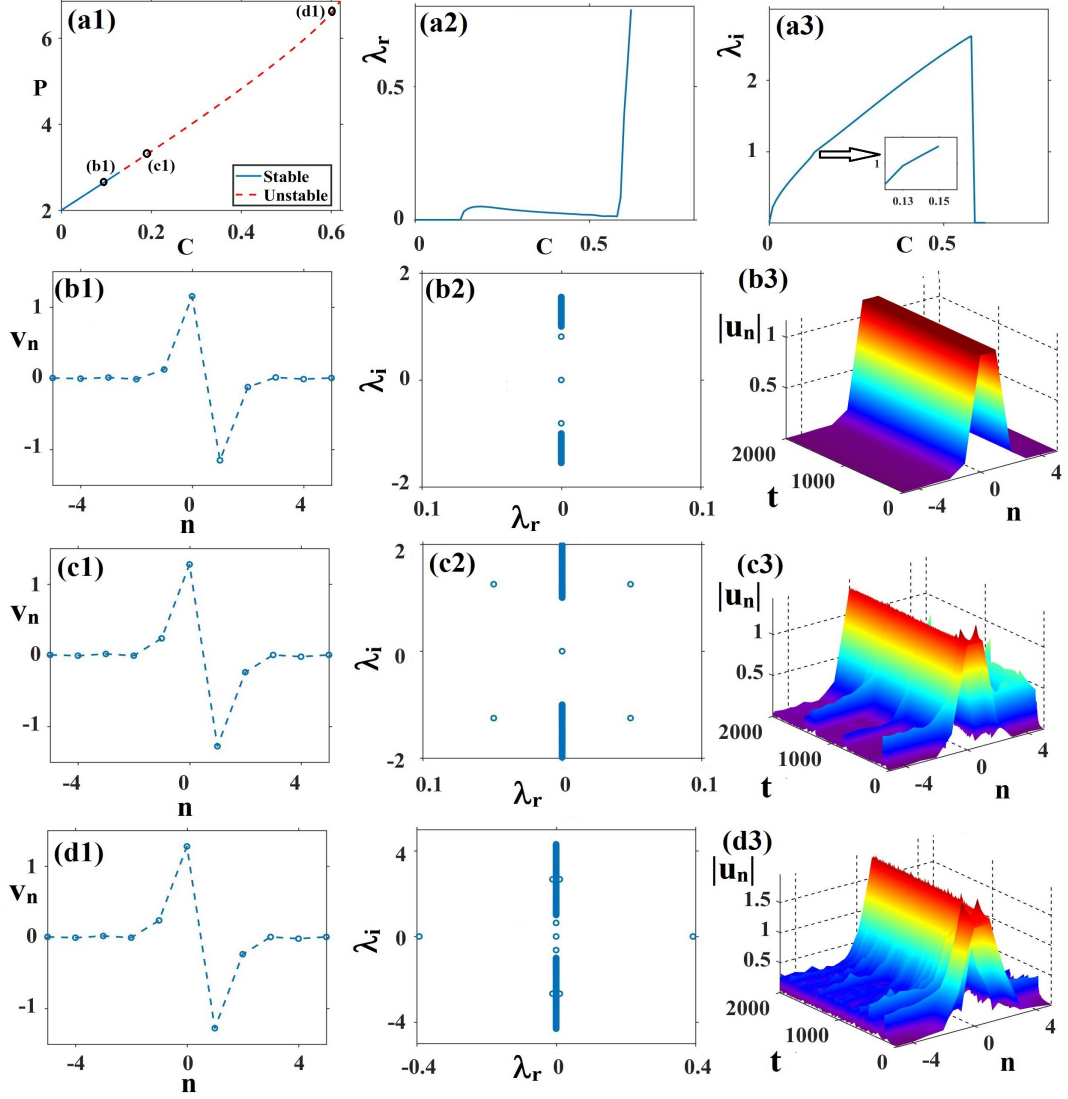


FIG. 5: Two-site out-of-phase modes at $\alpha = 1.5$. (a1) Power P vs. the coupling constant C , as produced by the numerical solutions of Eq. (26). The solid and dashed lines represent stable and unstable discrete solitons, respectively. Labels (b1,c1,d1) correspond to the discrete solitons displayed in panels (b1,c1,d1), respectively. (a2,a3) Critical eigenvalues (including real and imaginary parts) produced by the numerical solution of Eq. (29). The second row of panels display the profile of a discrete soliton for $C = 0.1$: (b1), the corresponding spectrum of perturbation eigenvalues (b2), and the evolution of the discrete soliton (b3). The third and fourth rows show the same as the second one, but for $C = 0.2$ and $C = 0.6$, respectively.

tween them, the emerging modes may be categorized as in-phase (alias offsite-centered, alias symmetric) and out-of-phase (alias twisted [81], i.e., antisymmetric) ones.

The results for the in-phase double-site mode produced at $\alpha = 1.5$ are represented in Fig. 4(a1) in the form of the $P(C)$ dependence. Similarly to the single-site excitation, the curve cannot continue up to the continuum limit, terminating at a critical value of the coupling constant C , which is the same as for the family of the single-site (onsite-centered) modes. Profiles of the double-site discrete soliton are displayed, as a function of C , in Fig. 4(a2), where the amplitude and width increase

with the growth of C . Like in the usual DNLS equation, the transition which breaks the symmetry between the two sites leads to a bifurcation of the translation eigenvalues from the origin to the real axis, rendering the corresponding discrete solitons linearly unstable. In contrast to the single-site excitation explored above, these eigenvalues branch out from the origin, rather than from the edge of the continuous spectrum, as can be explicitly seen in the AC limit. The variation of the critical eigenvalues with respect to C is presented in Figs. 4(a3,a4).

The in-phase two-site mode is made unstable by a real positive eigenvalue at all values of $C \neq 0$. As C in-

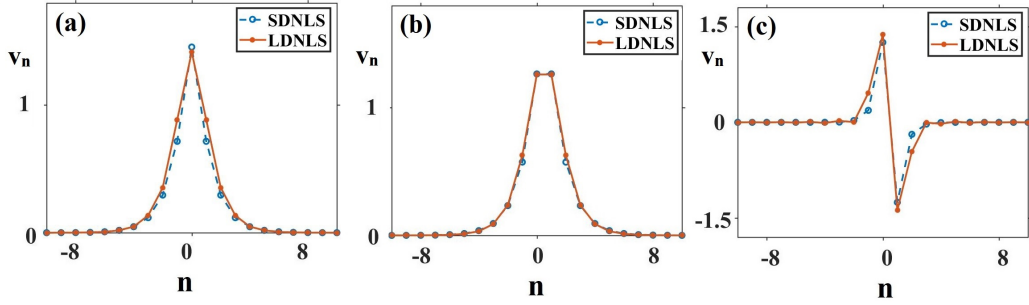


FIG. 6: Comparison of different discrete soliton profiles for DNLS equation (23) with long-range interactions (labeled as LDNLS with solid line), and for the usual short-range DNLS equation (24) (labeled as SDNLS with dashed line): (a) and (b) represent, respectively, the onsite- and offsite-centered solitons at $C = 1$; (c) represents twisted solitons at $C = 0.2$.

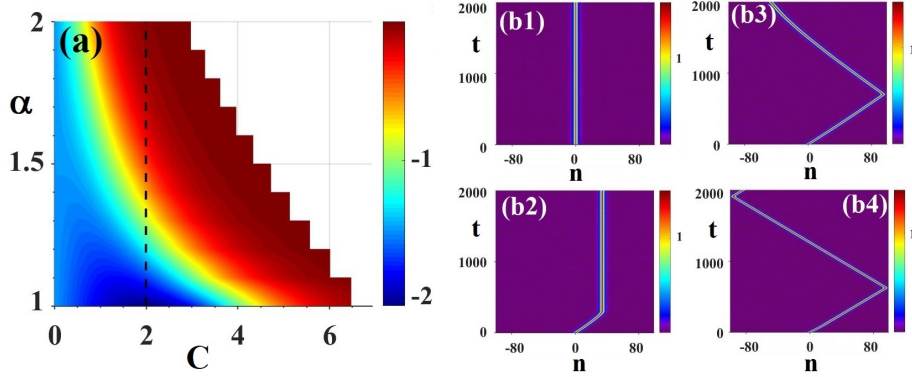


FIG. 7: (a) The magnitude of the Peierls-Nabarro barrier, ΔG , estimated as per Eq. (42), is shown in the (C, α) plane. The evolution of the discrete soliton initiated by kick $K = \pi/64$ (see Eq. (44)), for $C = 0.2$ and $\alpha = 1.5$ (b1), $\alpha = 1.7$ (b2), $\alpha = 1.8$ (b3), and $\alpha = 2.0$ (b4).

creases further, a pair of eigenvalues branches off from the edge of the continuous spectrum along the imaginary axis to form a point spectrum. Simultaneously, the unstable eigenvalues are decreasing in their magnitude. An example of an in-phase discrete soliton is displayed in Fig. 4(b1) for $C = 1$. Figure 4(b2) demonstrates that this discrete soliton is indeed linearly unstable, due to the bifurcation from the origin, cf. Refs. [57, 68, 70]. Direct simulations confirm the instability of this discrete soliton, see Figs. 4(b3,b4).

For the family of out-of-phase two-site (twisted) modes, the $P(C)$ dependence is presented in Fig. 5(a1), fixing $\alpha = 1.5$. The variation of critical eigenvalues is illustrated in Figs. 5(a2,a3). In this case, the translation eigenvalues bifurcate from the origin, and first move along the imaginary axis. Then, at $C \approx 0.14$, the collision with the edge of the continuous-spectrum band results in transformation of pure imaginary stability eigenvalues into a complex quartet. The latter effect is similar to the one known for the usual DNLS equation. This observation is explained by the fact that these eigenvalues have negative Krein signatures [57, 70], hence the collision gives rise to a complex quartet, through the

Hamilton-Hopf bifurcation [79, 80]. Thus, the family of the out-of-phase double-site discrete solitons, unlike its in-phase counterpart, contains the stable segment, as shown in Figs. 5(a1,a2). A different phenomenon is that, as found at $C \approx 0.6$, the eigenvalues bifurcating from the band edge of the continuous spectrum touch the origin and thus become real unstable eigenvalues. A stable discrete soliton is displayed in Fig. 5(b1) for $C = 0.1$, together with its spectrum of eigenvalues for small perturbations, and stable propagation in the direct simulations, see Figs. 5(b2,b3). When the coupling constant increases to $C = 0.2$, the discrete soliton exhibited in Fig. 5(c1) is linearly unstable due to complex eigenvalues, see Fig. 5(c2), as confirmed by the direct simulations in Fig. 5(c3). A linearly unstable discrete soliton is displayed in Fig. 5(d1) for $C = 0.6$, with the respective linear spectrum and unstable evolution exhibited in Figs. 5(d2) and (d3), respectively.

As said above, at $\alpha = 2$ our DNLS equation with long-range interactions, i.e., Eq. (23), does not reduce to the usual DNLS equation (24) with the short-range interaction, making it necessary to compare the two models. The results for different types of the discrete solitons

(onsite- and offsite-centered ones, as well as the twisted solitons) are summarized in Fig. 6, where one observes that both models actually produce very close results.

IV. MOBILITY AND COLLISIONS OF DISCRETE SOLITONS

In addition to the breaking of the invariance with respect to spatial displacements due to the discreteness, the Galilean invariance of the present system is broken by the fractional diffraction [31, 32], hence a nontrivial issue is mobility of initially kicked discrete solitons. As is well known, discrete solitons may move across a lattice if their kinetic energy exceeds the corresponding Peierls-Nabarro potential barrier (PNPB), which is usually estimated as the free-energy difference, $G = H - \omega P$, between the onsite- and offsite-centered modes [corresponding to subscripts “on” and “off” in Eq. (43)] for the same frequency ω or power P , i.e.,

$$\Delta G = \Delta H - \omega \Delta P, \quad (42)$$

where

$$\Delta H = H_{\text{off}} - H_{\text{on}}, \quad \Delta P = P_{\text{off}} - P_{\text{on}} \quad (43)$$

with the subscripts denoting the two-site in-phase and single-site mode, respectively [57, 77, 82–85]. The so generated estimate of the PNPB for the discrete soliton is presented in Fig. 7(a) in the (C, α) plane. As expected, the free energies of the onsite- and offsite-centered modes are close at larger C (as one approaches the continuum limit), and, as LI α decreases, a smaller difference of the free energies is observed for larger C . The prediction produced by PNPB was verified by simulating Eq. (16) with the initial input in the form of the stationary discrete soliton v_n , to which the kick k is applied:

$$u_n(t=0) = v_n e^{ikn}. \quad (44)$$

Several typical simulations are displayed in Figs. 7(b1–b4) for $k = \pi/64$. In Fig. 7(b1) one observes that the discrete soliton cannot be set in motion by the kick at $\alpha = 1.5$. At $\alpha = 1.7$ the application of the kick leaves the discrete soliton trapped after a period of transient motion. Persistently moving discrete solitons are observed in Figs. 7(b3,b4) for $\alpha = 1.9$ and 2.0, respectively, the motion being quicker in the latter case, which can be explained by the PNPB estimate in Fig. 7(a). Note that the moving discrete solitons bounce back from the boundary of the simulation domain.

It is natural too to simulate collisions between mobile discrete solitons moving in opposite directions, which are initialized by the input

$$u_n(0) = v_n^{+n_0} e^{ikn} + v_n^{-n_0} e^{-ikn}, \quad (45)$$

where $v_n^{\pm n_0}$ are quiescent discrete solitons with centers located at sites $n = \pm n_0$. Semi-elastic collisions are displayed in Figs. 8(a1,a2), for $\alpha = 1.7$ and 1.8, respectively. At $\alpha = 2$, the collision is inelastic, as seen in Fig. 8(a3).

Simulations clearly demonstrate that they lead to breaking of the symmetry of the two-soliton set. As explained earlier in terms of a continuum NLS equation with the non-fractional diffraction [86], the symmetry breaking in soliton-soliton collisions is not a spontaneous effect. In fact, it is a predictable one, caused by a mismatch between the amplitude and phase collision centers in the case of a soliton pair represented by a complex wave field.

V. CONCLUSIONS AND DISCUSSIONS

In the present work, we have proposed a novel form of the fractional discrete nonlinear Schrödinger equation, with Lévy index $\alpha \in (0, 2]$, based on the quasi-Riesz fractional derivative. In addition to the fractional case, with $\alpha < 2$, the case of $\alpha = 2$ also provides a new discrete nonlinear wave system with the long-range interaction decaying $\sim 1/l^2$ with the increase of distance l between sites of the dynamical lattice. A physical realization of the latter model is proposed, in terms of the array of parallel chains of atoms or molecules carrying permanent magnetic or electric dipole moments. The difference of the fractional discrete NLS equation obtained in the limit of $\alpha = 2$, with nonlocal inter-site couplings, from the usual discrete equation with the nearest-neighbor coupling is explained by the non-commutativity of the two transitions: $\alpha \rightarrow 2$ and proceeding from the continuum setting to the discrete lattice. The linear dispersion relation for linear waves in this FDNLS system is obtained.

Then, starting from the anti-continuous limit, the formation of discrete single- and double-site discrete solitons is investigated. The stability of the discrete solitons is examined by the calculation of eigenvalues for small perturbations, and is verified by means of direct simulations. Moreover, based on the free-energy estimates of the PNPB (Peierls-Nabarro barrier), mobility of the discrete solitons is predicted and tested in direct simulations. The simulations are also used to study collisions between the moving discrete solitons.

The present study suggests directions for further work. One aspect is that discrete solitons do not persist in the continuum limit due to long-range interaction. A detailed analysis of how the existence of the discrete solitons terminates as the continuum limit is approached would be relevant to perform. As briefly mentioned above, the present discrete system with the long-range intersite interactions may be naturally generalized by considering spatially periodic modulation of the interactions.

Another natural option is to consider nonlinear modes of other types, such as dark solitons [87, 88], surface

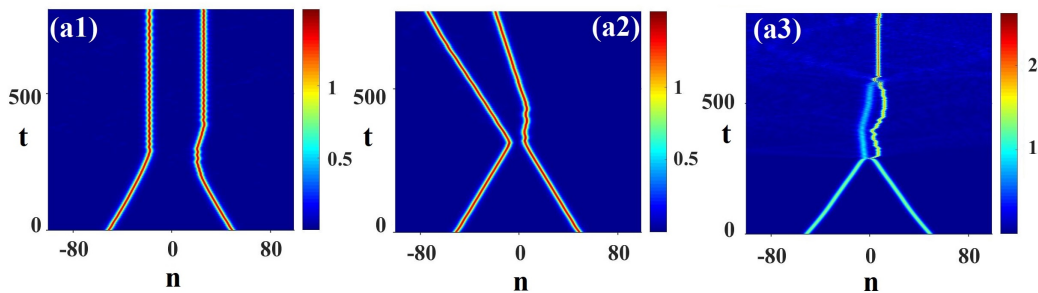


FIG. 8: Collisions between one-site discrete solitons, initially located at $n = \pm 50$, which are set in motion by kicks $k = \pm\pi/64$ for $\alpha = 1.7$ (a1), $\alpha = 1.8$ (a2), and $\alpha = 2.0$ (a3).

waves [89], etc. A challenging extension is to introduce a 2D version of the system and address modes such as 2D fundamental and vortex solitons. Further, as concerns physically relevant 2D settings, an intriguing possibility is to introduce a semi-discrete system (cf. Ref. [90]) described by the fractional NLS equation

$$i\partial_z u_n = \frac{1}{2} \left[\left(-\frac{\partial^2}{\partial x^2} \right)^{\alpha/2} + \left(-\frac{\widehat{\partial}^2}{\widehat{\partial} n^2} \right)^{\beta/2} \right] u_n + F(x, n, |u_n|^2) u_n, \quad (46)$$

where x and n are continuous and discrete coordinates,

respectively, with the corresponding Lévy indices α and β , the continuous and discrete fractional derivatives are defined, severally, as per Eqs. (4) and (9), and F represents a general nonlinear term. Such studies are currently in progress and will be reported elsewhere.

Acknowledgments

The work of Z.Y. was supported by the National Natural Science Foundation of China (No. 11925108). The work of B.A.M. is supported, in part, by grant No. 1695/22 from the Israel Science Foundation.

-
- [1] V. V. Uchaikin, *Fractional Derivatives for Physicists and Engineers* (Springer, New York, 2013).
- [2] M. Caputo, Linear model of dissipation whose Q is almost frequency independent. II, *Geophys. J. Inter.* **13**, 529–539 (1967).
- [3] M. F. Shlesinger, G. M. Zaslavsky, and J. Klafter, Strange kinetics, *Nature (London)* **363**, 31 (1993).
- [4] N. C. Petroni and M. Pusterla, Lévy processes and Schrödinger equation, *Physica A* **388**, 824 (2009).
- [5] N. Laskin, Fractional quantum mechanics, *Phys. Rev. E* **62**, 3135 (2000).
- [6] N. Laskin, Fractional quantum mechanics and Lévy path integrals, *Phys. Lett. A* **268**, 298–305 (2000).
- [7] N. Laskin, Fractional Schrödinger equation, *Phys. Rev. E* **66**, 056108 (2002).
- [8] P. Barthelemy, J. Bertolotti, and D. S. Wiersma, A Lévy flight for light, *Nature* **453**, 495–8 (2008).
- [9] N. Mercadier, W. Guerin, M. Chevrollier, and R. Kaiser, Lévy flights of photons in hot atomic vapours, *Nat. Phys.* **5**, 602–605 (2009).
- [10] B.A. Stickler, Potential condensed-matter realization of space-fractional quantum mechanics: the one-dimensional Lévy crystal, *Phys. Rev. E* **88**, 012120 (2013).
- [11] M. I. Molina, Fractionality and PT symmetry in a square lattice, *Phys. Rev. A* **106**, L040202 (2022).
- [12] S. Kumar, P. Li, and B. A. Malomed, Domain walls in fractional media, *Phys. Rev. E* **106**, 054207 (2022).
- [13] G. Samorodnitsky and M. S. Taqqu, *Stable Non-Gaussian Random Processes* (Chapman and Hall, New York, 1994).
- [14] N. Laskin, *Fractional Quantum Mechanics* (World Scientific: Singapore, 2018).
- [15] S. G. Samko, A. A. Kilbas, and I. O. Marichev, *Fractional Integrals and Derivatives: Theory and Applications* (Gordon and Breach, 1993).
- [16] R. Hilfer, *Applications of fractional calculus in physics* (World Scientific, Singapore, 2000).
- [17] C. A. Monje, Y. Q. Chen, B. M. Vinagre, D. Xue, and V. Feliu, *Fractional-order systems and controls* (Springer, Berlin, 2010).
- [18] V. E. Tarasov, *Fractional dynamics: applications of fractional calculus to dynamics of particles, fields and media* (Springer, Berlin 2011).
- [19] V. Uchaikin and R. Sibatov, *Fractional kinetics in solids: Anomalous charge transport in semiconductors, dielectrics and nanosystems* (World Scientific Publishing, Singapore, 2013).
- [20] R. Metzler and J. Klafter, The random walk’s guide to anomalous diffusion: a fractional dynamics approach, *Phys. Rep.* **339**, 1–77 (2000).
- [21] G. M. Zaslavsky, Chaos, fractional kinetics, and anomalous transport, *Phys. Rep.* **371**, 461 (2002).
- [22] H. Sun, Y. Zhang, D. Baleanu, W. Chen, and Y. Chen, A new collection of real world applications of fractional calculus in science and engineering, *Commun. Nonlinear*

- Sci. Numer. Simulat. **64**, 213-231 (2018).
- [23] X. Guo and M. Xu, Some physical applications of fractional Schrödinger equation, *J. Math. Phys.* **47**, 082104 (2006).
- [24] B. B. Mandelbrot, *The Fractal Geometry of Nature* (W. H. Freeman, New York, 1982).
- [25] S. Albeverio, R. Hoegh-Krohn, and S. Mazzucchi, *Mathematical Theory of Feynman Path Integrals : An Introduction* (Springer, Berlin and Heidelberg, 2008).
- [26] S. Longhi, Fractional Schrödinger equation in optics, *Opt. Lett.* **40**, 1117-1120 (2015).
- [27] Y. Zhang, X. Liu, M. R. Belić, W. Zhong, Y. Zhang, and M. Xiao, Propagation dynamics of a light beam in a fractional Schrödinger equation, *Phys. Rev. A* **115**, 180403 (2015).
- [28] W. P. Zhong, M. R. Belić, B. A. Malomed, Y. Zhang, and T. Huang, Spatiotemporal accessible solitons in fractional dimensions, *Phys. Rev. E* **94**, 012216 (2016).
- [29] Y. Zhang, H. Zhong, M. R. Belić, Y. Zhu, W. Zhong, Y. Zhang, D. N. Christodoulides, and M. Xiao, PT-symmetry in a fractional Schrödinger equation, *Laser Photonics Rev.* **10**, 526-531 (2016).
- [30] M. Cai and C. P. Li, On Riesz derivative, *Fractional Cal. Appl. Anal.* **22**, 287-301 (2019).
- [31] B. A. Malomed, Optical solitons and vortices in fractional media: A mini-review of recent results, *Photonics* **8**, 353 (2021).
- [32] B. A. Malomed, Basic fractional nonlinear-wave models and solitons, *Chaos*, in press.
- [33] V. A. Stephanovich , E. V. Kirichenko , G. Engel , and A. Sinner, Spin-orbit-coupled fractional oscillators and trapped Bose-Einstein condensates, *Phys. Rev. E* **109**, 014222 (2024).
- [34] L. P. Pitaevskii and S. Stringari, *Bose-Einstein Condensation* (Oxford University Press, Oxford, 2003).
- [35] C. Huang, H. Deng, W. Zhang, F. Ye, and L. Dong, Fundamental solitons in the nonlinear fractional Schrödinger equation with a PT-symmetric potential, *EPL* **122**, 24002 (2008).
- [36] C. Huang and L. Dong, Gap solitons in the nonlinear fractional Schrödinger equation with an optical lattice, *Opt. Lett.* **41**, 5636-5639 (2016).
- [37] L. Zhang, C. Li, H. Zhong, C. Xu, D. Lei, Y. Li, and D. Fan, Propagation dynamics of super-Gaussian beams in fractional Schrödinger equation: from linear to nonlinear regimes, *Opt. Exp.* **24**, 14406-14418 (2016).
- [38] X. Yao and X. Liu, Off-site and on-site vortex solitons in space-fractional photonic lattices, *Opt. Lett.* **43**, 5749-5752 (2018).
- [39] M. Chen, S. Zeng, D. Lu, W. Hu, and Q. Guo, Optical solitons, self-focusing, and wave collapse in a space-fractional Schrödinger equation with a Kerr-type nonlinearity, *Phys. Rev. E* **98**, 022211 (2018).
- [40] L. Zeng and J. Zeng, Preventing critical collapse of higher-order solitons by tailoring unconventional optical diffraction and nonlinearities, *Commun. Phys.* **3**, 26 (2020).
- [41] J. Xie, X. Zhu, and Y. He, Vector solitons in nonlinear fractional Schrödinger equations with parity-time-symmetric optical lattices, *Nonlinear Dyn.* **97**, 1287 (2019).
- [42] P. Li, B. A. Malomed, and D. Mihalache, Symmetry-breaking bifurcations and ghost states in the fractional nonlinear Schrödinger equation with a PT-symmetric potential, *Opt. Lett.* **46**, 3267 (2021).
- [43] M. Zhong, L. Wang, P. Li, and Z. Yan, Spontaneous symmetry breaking and ghost states supported by the fractional PT-symmetric saturable nonlinear Schrödinger equation, *Chaos* **33**, 013106 (2023).
- [44] M. Zhong, Y. Chen, Z. Yan, and B. A. Malomed, Suppression of soliton collapses, modulational instability and rogue-wave excitation in two-Lévy-index fractional Kerr media, *Proc. R. Soc. A* **480**, 20230765 (2024).
- [45] C. Klein, C. Sparber, and P. Markowich, Numerical study of fractional nonlinear Schrödinger equations, *Proc. R. Soc. A* **470**, 20140364 (2014).
- [46] Y. S. Kivshar and G. P. Agrawal, *Optical Solitons: From Fibers to Photonic Crystals* (Academic Press, San Diego, 2003).
- [47] S. Liu, Y. Zhang, B. A. Malomed, and E. Karimi, Experimental realisations of the fractional Schrödinger equation in the temporal domain, *Nature Comm.* **14**, 222 (2023).
- [48] Y. B. Gaididei, S. F. Mingaleev, P. L. Christiansen, and K. Ø. Rasmussen, Effects of nonlocal dispersive interactions on self-trapping excitations, *Phys. Rev. E* **55**, 6141 (1997).
- [49] M. Jenkinson, and M. I. Weinstein, Discrete solitary waves in systems with nonlocal interactions and the Peierls-Nabarro barrier, *Commun. Math. Phys.* **351**, 45-94 (2017).
- [50] O. Ciaurri, L. Roncal, P. R. Stinga, J. L. Torrea, and J. L. Varona, Nonlocal discrete diffusion equations and the fractional discrete Laplacian, regularity and applications, *Adv. Math.* **330**, 688-738 (2018).
- [51] M. I. Molina, The fractional discrete nonlinear Schrödinger equation, *Phys. Lett. A* **384**, 126180 (2020).
- [52] M. I. Molina, The two-dimensional fractional discrete nonlinear Schrödinger equation, *Phys. Lett. A* **384**, 126835 (2020).
- [53] M. I. Molina, Fractional nonlinear electrical lattice, *Phys. Rev. E* **104**, 024219 (2021).
- [54] V. E. Tarasov, Continuous limit of discrete systems with long-range interaction, *J. Phys. A: Math. Gen.* **39**, 14895 (2006).
- [55] V. E. Tarasov, Map of discrete system into continuous, *J. Math. Phys.* **47** 092901 (2006).
- [56] V. E. Tarasov, Exact discretization by Fourier transforms, *Commun. Nonlinear Sci. Numer. Simul.* **37**, 31-61 (2016).
- [57] P. G. Kevrekidis, *The discrete nonlinear Schrödinger equation: mathematical analysis, numerical computations and physical perspectives* (Springer, Berlin, 2009).
- [58] J. C. Eilbeck, P. S. Lomdahl, and A. C. Scott, The discrete selftrapping equation, *Physica D* **16**, 318-338 (1985).
- [59] F. Lederer, G. I. Stegeman, D. N. Christodoulides, G. Assanto, M. Segev, and Y. Silberberg Discrete solitons in optics, *Phys. Rep.* **463**, 1-126 (2008).
- [60] L. N. Trefethen, *Spectral methods in MATLAB* (SIAM, 2000).
- [61] K. Atkinson, *An Introduction to Numerical Analysis* (John Wiley & Sons, New York, 1991).
- [62] T. Lahaye, C. Menotti, L. Santos, M. Lewenstein, and T. Pfau, The physics of dipolar bosonic quantum gases, *Rep. Prog. Phys.* **72**, 126401 (2009).
- [63] H. Sakaguchi and B. A. Malomed, Suppression of the quantum-mechanical collapse by repulsive interactions in a quantum gas, *Phys. Rev. A* **83**, 013607 (2011).

- [64] R. S. MacKay, and S. Aubry, Proof of existence of breathers for time-reversible or Hamiltonian networks of weakly coupled oscillators, *Nonlinearity* **7**, 1623 (1994).
- [65] S. Aubry, Breathers in nonlinear lattices: Existence, linear stability and quantization, *Physica D* **103**, 201-250 (1997).
- [66] D. Hennig and G. P. Tsironis, Wave transmission in nonlinear lattices, *Phys. Rep.* **307**, 333-432 (1999).
- [67] H. R. Dullin and J. D. Meiss, Generalized Hénon maps: the cubic diffeomorphisms of the plane, *Physica D* **143**, 262-289 (2000).
- [68] T. Kapitula and P. Kevrekidis, Stability of waves in discrete systems, *Nonlinearity* **14**, 533 (2001).
- [69] G. L. Alfimov, V. A. Brazhnyi, and V. V. Konotop, On classification of intrinsic localized modes for the discrete nonlinear Schrödinger equation, *Physica D* **194**, 127-150 (2004).
- [70] D. E. Pelinovsky, P. G. Kevrekidis, and D. J. Frantzeskakis, Stability of discrete solitons in nonlinear Schrödinger lattices, *Physica D* **212**, 1-19 (2005).
- [71] H. Levy and F. Lessman, *Finite Difference Equations* (Courier Corporation, 1992).
- [72] R. A. Horn and C. R. Johnson, *Matrix Analysis* (Cambridge University Press, Cambridge, 2012).
- [73] J. Catarecha, J. Cuevas-Maraver, and P. G. Kevrekidis, Breathers in the fractional Frenkel-Kontorova model, arXiv:2311.01809 (2023).
- [74] S. Flach, Breathers on Lattices with Long Range Interaction, *Phys. Rev. E* **58**, R4116 (1998).
- [75] M. Stepić, D. Kip, L. Hadzievski, and A. Maluckov, One-dimensional bright discrete solitons in media with saturable nonlinearity, *Phys. Rev. E* **69**, 066618 (2004).
- [76] L. Hadzievski, A. Maluckov, M. Stepić, and D. Kip, Power controlled soliton stability and steering in lattices with saturable nonlinearity, *Phys. Rev. Lett.* **93**, 033901 (2004).
- [77] T. R. Melvin, A. R. Champneys, P. G. Kevrekidis, and J. Cuevas, Radiationless traveling waves in saturable nonlinear Schrödinger lattices, *Phys. Rev. Lett.* **97**, 124101 (2006).
- [78] M. Johansson, and S. Aubry, Growth and decay of discrete nonlinear Schrödinger breathers interacting with internal modes or standing-wave phonons, *Phys. Rev. E* **61**, 5864 (2000).
- [79] J. C. van der Meer, Hamiltonian Hopf bifurcation with symmetry, *Nonlinearity* **3**, 1041 (1990).
- [80] R. S. MacKay, Movement of eigenvalues of Hamiltonian equilibria under non-Hamiltonian perturbation, *Phys. Lett. A* **155**, 266-268 (1991).
- [81] S. Darmanyan, A. Kobayakov, and F. Lederer, Stability of strongly localized excitations in discrete media with cubic nonlinearity, *Zh. Eksp. Teor. Fiz.* 113, 1253-1260 (1998) [*J. Exp. Theor. Phys.* **86**, 682-686 (1998)].
- [82] Y. S. Kivshar and D. K. Campbell, Peierls-Nabarro potential barrier for highly localized nonlinear modes, *Phys. Rev. E* **48**, 3077-3081 (1993).
- [83] D. Cai, A. R. Bishop, and N. Grønbech-Jensen, Localized states in discrete nonlinear Schrödinger equation, *Phys. Rev. Lett.* **72**, 591-595 (1994).
- [84] R. Morandotti, U. Peschel, J. S. Aitchison, H. S. Eisenberg, and Y. Silberberg, Dynamics of discrete solitons in optical waveguide arrays, *Phys. Rev. Lett.* **83**, 2726-2729 (1999).
- [85] A. Maluckov, L. Hadzievski, and B. A. Malomed, Staggered and moving localized modes in dynamical lattices with the cubic-quintic nonlinearity, *Phys. Rev. E* **77**, 036604 (2008).
- [86] L. Khaykovich and B. A. Malomed, Deviation from one dimensionality in stationary properties and collisional dynamics of matter-wave solitons, *Phys. Rev. A* **74**, 023607 (2006).
- [87] Y. S. Kivshar, W. Królikowski, and O. A. Chubykalo, Dark solitons in discrete lattices, *Phys. Rev. E* **50**, 5020 (1994).
- [88] E. P. Fitrakis, P. G. Kevrekidis, H. Susanto, and D. J. Frantzeskakis, Dark solitons in discrete lattices: Saturable versus cubic nonlinearities, *Phys. Rev. E* **75**, 066608 (2007).
- [89] K. G. Makris, S. Suntsov, D. N. Christodoulides, G. I. Stegeman, and A. Hache, Discrete surface solitons, *Opt. Lett.* **30**, 2466-2468 (2005).
- [90] X. Zhang, X. Xu, Y. Zheng, Z. Chen, B. Liu, C. Huang, B. A. Malomed, and Y. Li, Semidiscrete quantum droplets and vortices, *Phys. Rev. Lett.* **123**, 133901 (2019).